75th International Astronautical Congress (IAC), Milan, Italy, 14-18 October 2024.

IAC–24–C1.8.9

Investigating (65803) Didymos properties and dynamical evolution as an N-body system

Giorgia Rota[a*], **Fabio Ferrari**[b]

[a] *Department of Aerospace Science and Technology, Politecnico di Milano, Via La Masa 34, 20156 Milano, Italy, giorgia.rota@mail.polimi.it*
[b] *Department of Aerospace Science and Technology, Politecnico di Milano, Via La Masa 34, 20156 Milano, Italy, fabio1,ferrari@polimi.it*
[*] *Corresponding author*

Abstract

The dynamics governing asteroids, particularly those exhibiting traits of rubble-piles, remain a compelling and open area of research. This complexity arises from the challenges associated with analysing the interactions between their components, along with the numerous factors and constraints that can influence their evolutionary trajectories. This research delves into the dynamics and characterization of rubble-pile asteroids, focusing on the case of asteroid (65803) Didymos. The asteroid's dynamical behaviour is addressed, specifically exploring the influence of its properties and internal structure on its evolution as an N-body system undergoing gravitational interactions and contacts. The main objective of this research is to establish correlations between Didymos's properties, such as shape and mass distribution, and its dynamical evolution. Additionally, the potential existence of a rigid core within Didymos's rubble-pile structure is explored. A numerical approach is carried out using the GRAINS N-body DEM code. Diverse models of Didymos, ranging from those with a rigid core to more homogeneous aggregates, are considered. The simulations explore the impact of a defined internal volume's density on the asteroid's long-term evolution, providing a controlled environment to collect data. The effects of different configurations on the asteroid's gravitational interactions are presented through rigorous post-processing of the significant parameters related to aggregate evolution. The results obtained reveal that a rigid core significantly influences the final configuration, providing insights into the dynamical evolution of rubble-pile asteroids. The core stabilizes the system, reducing asymmetrical deformations and mass losses, and introducing distinctive features. In addition, the movement of the system's barycenter is found to affect the inner particles of the aggregate. Thus, this work contributes to advancing rubble-pile asteroid knowledge, improving predictions that aid mission planning and Earth's defense against impact threats, relevant to upcoming missions like ESA's Hera.

1. Introduction

Asteroids, fundamental constituents of the solar system's minor bodies alongside comets, meteoroids, and interplanetary dust, form a diverse population characterized by variable sizes and compositions. Since asteroids were first discovered in 1801, over 750,000 of these celestial bodies have been cataloged, revealing a dynamic array of shapes and sizes [1]. Observations, facilitated mainly by telescopes due to their faintness, have disclosed irregular, crater-covered surfaces with regolith and pulverized rock. Asteroids are not only classified based on composition but also by their locations within the solar system, with prevailing theories suggesting concurrent formation with major planets. The Main Asteroid Belt, between Mars and Jupiter, hosts the largest concentration of asteroids, while Trojan Asteroids and Near-Earth Asteroids (NEAs) form significant subsets of this population. NEAs, in particular, have garnered extensive attention for their implications in planetary defense [2]. Comprehensive research efforts, notably through initiatives like NASA's Near-Earth Object Program [3] and collaborative missions such as ESA's Hera with NASA's DART, aim to understand NEAs' characteristics and enhance planetary defense capabilities. Specifically, the (65803) Didymos binary asteroid system, comprising the primary body Didymos and its moonlet Dimorphos, serves as a focal point for scientific inquiry and planetary defense strategies. The AIDA mission, involving DART and Hera, successfully assessed the feasibility of deflecting Dimorphos through kinetic impact [4] and is expected to provide distinctive information regarding the strength, surface properties and internal structure of these asteroids.

This research focuses on studying the primary asteroid in the Didymos binary system, aiming to correlate the asteroid's properties, like internal configuration and mass distribution, with its dynamical evolution. Furthermore, the existence of a rigid core within its rubble-pile structure is explored. Thus, numerical simulations are employed to evaluate the complex dynamics characterizing rubble-pile asteroids, offering further insights into granular dynamics

evolution and enhancing understanding in the planetary defense context. Through a comprehensive literature review, theoretical framework, and rigorous results analysis, this study intends to contribute to the growing knowledge of asteroid dynamics and provide information for future efforts in planetary defense and space exploration.

2. Rubble-pile Asteroids

Rubble-pile asteroids consist of rocky and metallic fragments forming an unorganized collection loosely held together by gravity. Characterized by minimal tensile strength and moderate bulk porosity, these asteroids feature significant internal voids [5].

Numerical simulations revealed that the internal cohesion of rubble-pile asteroids significantly influences their behaviour during spin-up, with cohesive forces affecting the disruption process and fragment sizes [6]. Thus, increased cohesive strength reduces deformation before disruption, leading to abrupt fragmentation, potentially forming asteroid pairs or active asteroids. Furthermore, granular N-body simulations have been used alongside theoretical frameworks to decode particle-scale dynamics and transitions. This investigation in the density-spin parameters space led to the identification of breakup limits and reshape regions [7].

2.1 Past missions: asteroids Bennu and Ryugu

Two top-shaped asteroids, (101955) Bennu and (162173) Ryugu, have been subjects of detailed scientific investigation during past missions. However, due to the inability to directly probe their interiors, numerical simulations were crucial for understanding their geophysical characteristics, relying solely on interpreting external properties. Bennu's sensitivity to material strength was revealed through spin-up studies, indicating low-cohesion structures with cohesive internal zones, suggesting the presence of large boulders or cohesive grains [8]. Comparisons with constant-density models revealed heterogeneous mass distribution, with lower densities at the equatorial bulge and center [9]. Moreover, increased spin rates were found to cause material migration into the external equatorial region.

In Ryugu's case, its irregularity hints at varied clast arrangements with low cohesion and its smooth western bulge indicates stable subsurface structure and asymmetric deformation [10].

2.2 Numerical studies on Didymos

This binary system has been mostly studied in relation to its selection for the DART and Hera missions to evaluate its structural response to kinetic impact. Some numerical studies on Didymos suggested factors, such as cohesion or higher density than estimated, contributing to its surface stability [11]. These findings supported hypotheses linking fast rotation to equatorial ridge formation.

However, since local surface sampling of top-shaped NEAs revealed porous structures with minimal strength and cohesion [12], the presence of a mechanically resistant core in Didymos was investigated. This idea was initially explored using an SSDEM capable of simulating granular systems, where Didymos, simulated as a crystalline structure with high friction or as a random packing with a higher-density core, may reach stability acting as a rigid core with a weak surface envelope [13].

Additionally, numerical simulations using GRAINS N-body DEM code were carried out involving irregular rocky fragments aggregates with a rigid core [14]. These show that a higher percentage of internal rigidity corresponds to greater surface and shape irregularities, preventing internal collapse and facilitating significant surface movement. Thus, surface cohesion may not be essential for stability in top-shaped rubble-pile asteroids with a certain level of internal rigidity.

3. Principles of Granular Mechanics

Gravitational interactions within celestial dynamics necessitate a meticulous examination of energy requirements and stability considerations. Understanding gravitational forces involves studying gravitational potential energy, kinetic energy, angular momentum and their implications for celestial body stability.

3.1 Discrete particle systems analysis and Hill Stability

Departing from traditional point-mass methods, a shift towards a more realistic portrayal of celestial bodies emerged, acknowledging a finite-density approach and consequent behavioral implications [15]. Fundamental to celestial mechanics are two conservation principles: momentum and energy, which typically remain constant in isolated systems but are challenged by real-world dissipation phenomena. This requires consideration of the minimum energy configuration for N-body systems with fixed angular momentum, a challenge addressed by the Full N-Body Problem [15]. This comprehensive approach incorporates finite-density and rotational motion modeling, refining knowledge of minimum energy configurations. Furthermore, delving into Hill Stability and disruption energy offers crucial insights for evaluating system stability and dynamics [16]. The Hill Stability Theorems establish conditions ensuring stability, setting a critical benchmark for identifying disruptive energy levels and assessing configuration stability.

For instance, in spherical N-body systems, stability is achieved when total energy falls below the minimum po-

tential energy across all possible relative configurations for an N-1 body system [16]. Increasing system energy makes certain configurations prone to disruption, while others remain stable, with configurations involving more bodies typically requiring lower energy levels for stability. This dynamic interplay underscores the stability dynamics within N-body systems, highlighting the resilience of certain configurations, such as equal mass resting configurations, even during fission processes.

3.2 Granular configurations stability

In exploring granular configurations and stability dynamics, dissipation parameters and angular momentum deeply influence system configurations. In the context of the sphere-restricted planar three-body problem, three main end states are identified: the Lagrange, the variable and the Euler resting configurations. Extending the Euler Resting configuration's stability analysis to N-body cases reveals the configuration's stability up to five bodies, beyond which instability prevails [17]. Spin rates also play a critical role, determining system stabilization thresholds and fission points, particularly at higher angular momentum levels where centrifugal forces induce system separation.

Additionally, examining aggregate evolution, three main conditions can be achieved depending on the system-level constraints: reconfigurations, fission, or catastrophic disruptions [18]. Thus, critical spin rates and energy requirements are employed to delineate system fission and subsequent stability, revealing a direct correlation between system stability and the distribution of mass within the rubble-pile components.

Another crucial aspect is the investigation of dissociation energies between various size distributions. Although asteroids of identical mass and largest size boulders are compared directly, variations in size distribution and porosity can lead to significant changes in the overall configurations of these bodies [19].

Therefore, this rigorous framework offers an overview of the implications of energy requirements, providing insights into the gravitational interaction effects driving the evolution of rubble-pile asteroids. However, chaotic dynamics and instability are embedded in asteroids' behaviour [7], with small perturbations in initial conditions growing exponentially in self-gravitating N-body systems, particularly evident in larger systems. Thus, the effects of various factors need to be addressed for a more complete analysis, including the arrangement and size distribution of constituent particles, bulk density and interparticle friction.

4. Methodology

The previous sections presented the complex dynamics of N-body systems, necessitating numerical simulations due to the lack of analytical solutions. Discrete Element Methods are preferred for modeling granular materials, despite their computational demands. Thus, the GRAINS code [20] was selected for its ability to model cohesionless aggregates with irregularly shaped particles, improving the realism of simulations.

4.1 GRAINS: an N-body DEM code

GRAINS [21] is an N-body code, fully integrated with the multi-physics engine Chrono and implemented to study gravitational aggregates by handling both gravity and contact dynamics between complex-shaped objects.

The structure of the GRAINS code features interchangeable units of software known as modules. Each module encapsulates specific methods and routines tailored to execute distinct tasks within the simulation framework. The primary modules, either developed or directly retrieved from C::E libraries, include gravity, contact, rigid-body dynamics, body creation, numerical solvers, data input/output, visual interface and post-processing. The data input/output interface allows for the assignment of user-tunable parameters through an input text file, while output data are conveniently saved into dedicated text files.

Two main approaches are employed in simulating the gravitational aggregation problem: the classical N-body problem with point-mass sources and the hierarchical treecode algorithm. Thus, to overcome computational inefficiencies inherent in the direct N^2 method, the Barnes–Hut algorithm is also employed, significantly reducing time complexity to $O(N \log(N))$ and enabling more efficient simulations even with larger numbers of bodies. The creation of bodies and the definition of their inertial and surface properties can be handled by the user, selecting shapes from common geometries or custom meshes. Each body has six degrees of freedom, enabling translational and rotational motion. This flexibility in modeling ensures precise and controlled numerical simulations.

4.2 Simulations workflow

To analyze the primary body within the Didymos binary system, the study focuses on its global shape, surface stability, and internal structure evolution as a cohesionless gravitational aggregate. An extensive campaign of 26 simulations featuring diverse internal structures and distinct physical properties was considered. This dataset is categorized into two batches: 13 simulations with a rigid internal core and 13 with a more homogeneous aggregate lacking internal rigidity. By varying the density of a defined internal volume while maintaining a fixed initial spin rate,

the study examines how the internal structure and density influence long-term evolution.

4.3 Didymos shape models

Two Didymos asteroid models are created using 3D models from DART mission data [22]. These serve as templates to shape the asteroid from a generic aggregate of fragments. Each particle within the system exhibits a non-spherical and irregular form. The unique shapes of individual fragments are randomly generated, as the convex envelope of a cloud of points, with about 12 vertices on average. The internal structure of the models differs:

- The two-layer rubble-pile of 5973 particles has an irregular-shaped internal rigid core occupying about 17% of the total volume, surrounded by smaller fragments.
- The homogeneous aggregate consists of a single layer of 6455 particles filling the entire volume.

These models are shown in Figure 1, positioned at the center of the inertial frame (x, y, z) used in the simulations. Their properties are reported in Appendix A. The particle count is chosen to balance computational effort and resolution for meaningful simulations. The model without a rigid core has a higher particle count, as smaller particles are required to occupy the core's volume, leading to increased material density to maintain constant bulk density due to higher inter-particle voids.

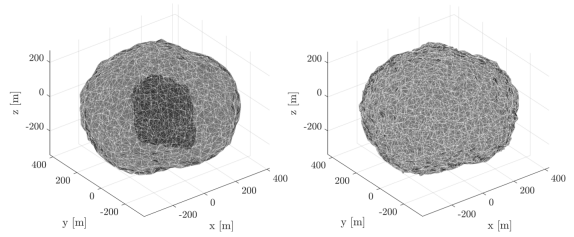

Fig. 1. Initial aggregates with and without the rigid core.

Additionally, the initial spin rate, set to a rotational period of $T = 2.26$ hours as in Table 1, and the surface properties of the aggregate are provided at the outset, see Appendix A.

Spin rate [rad/s]	Spin rate [deg/s]	Period [h]
7.7227×10^{-4}	4.4248×10^{-2}	2.26

Table 1. Initial spin condition.

4.4 Simulations campaign

The simulation campaign is designed to investigate the impact of altering internal density distributions within the rubble-pile structure. Thus, an internal volume of fragments is selected for the density variation while keeping the nominal density for the rest of the aggregate. For both sets of simulations three main cases are considered:

1. **Nominal Case**: The aggregate features a uniform density distribution.
2. **Denser Internal Volume Cases**: Six scenarios explore aggregates progressively increasing the density of the internal volume by +150 kg/m^3 for each case, up to a maximum increase of +900 kg/m^3.
3. **Underdense Internal Volume Cases**: Another set of six scenarios investigates aggregates gradually decreasing the density of the internal volume by -150 kg/m^3 for each case, reaching a maximum decrease of -900 kg/m^3.

For simulations with a rigid core (*C*), this implies changing only the rigid core density, while for the homogeneous aggregate (*N*) this means adjusting the density of all particles inside a comparable internal volume. The selected radius for this purpose is $r_{IC} = 122.4$ m, ensuring a variation comparable to that achieved with the rigid core. Notably, in the scenario with distinct layers, the density distribution is manipulated by varying the material density of individual particles, while maintaining a consistent overall bulk density.

Furthermore, the integration time-step alignment with system dynamics [20] is crucial for accurately representing gravitational interactions in numerical simulations. While gravitational interactions operate on a slow time scale, collisions introduce a significantly faster dynamic time scale, necessitating shorter time steps for precise, especially with complex object shapes. Thus, the selection of an appropriate time-step value is achieved empirically by evaluating the conservation of the total angular momentum of the system. To address this, shorter test simulations spanning 30 minutes are conducted, starting from nominal models, to assess errors effectively. Results indicate $\Delta t_g = 0.30\,s$ for the rigid core case and $\Delta t_g = 0.25\,s$ for the scenario without a rigid core. These values are selected for an extended 10-hour simulation campaign to comprehensively evaluate the aggregates' long-term evolution and dynamics.

Each simulation is uniquely identified by a specific ID based on the density variations being analyzed. In this system, the letter represents the shape model: *C* for the rigid core case and *N* for the non-rigid core case. The accompanying number denotes the density variation within

the aggregate, with 1 indicating the lowest density, 7 the nominal and 13 the highest. This identification method provides a quick and efficient way to reference both the shape model and corresponding density variations for each simulation.

5. Results Analysis

This chapter presents the outcomes of the simulations, with each section delving into distinct parameters of interest and elucidating the respective processing methods employed. Only selected results are presented here; for further details, please refer to the additional results provided in Appendix B.

5.1 Final shape configurations

The simulations conducted have provided valuable insights into the final configurations of the aggregates. The focus is on the nominal cases *C7* and *N7*, see Figures 2 and 3, taken as reference in the presentation of the results.

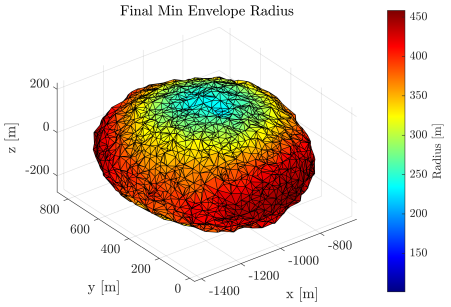

Fig. 2. **C7**: Final aggregate with a rigid core.

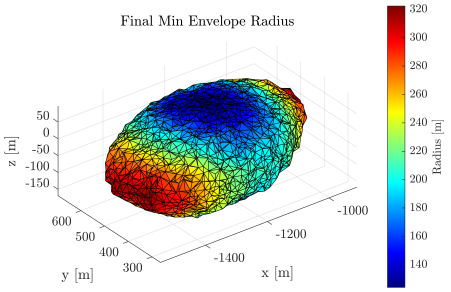

Fig. 3. **N7**: Final aggregate without a rigid core.

A key observation is the displacement of the aggregates' centers due to interactions between their internal structure and rotational dynamics. As shown in Figure 14, in scenarios with a rigid core, an increase in internal density correlates with a decrease in oblateness, indicating a trend toward a more spheroidal shape. Conversely, in scenarios without a rigid core, no explicit trend is observed, but an inverse correlation between oblateness and mass loss emerges, suggesting reduced flattening with greater mass loss.

Both aggregate configurations exhibit flattening at the poles, particularly pronounced in cases without a rigid core, where two bulges form at the equator, becoming focal points for mass loss. Despite asymmetry and deformations, aggregates reach equilibrium, with those without a rigid core tending towards a more elongated configuration. The presence of bulges is also observed in rigid core cases with an equatorial ridge, although less pronounced and without mass loss, indicating the stabilizing effect of the core.

Notably, simulations revealed a groove-like feature in the rigid core case, as shown in Figure 4. This distinctive feature crosses the aggregate within the longitude range of 150-300 degrees, likely resulting from the core's irregular structure. This observation could offer a valuable explanatory element for the presence of fossae on the surface of asteroids, establishing a connection with potential real asteroids, particularly if they exhibit a similar configuration. For instance, asteroid Bennu's shape and surface characteristics indicate a degree of structural rigidity, despite its rubble-pile composition [8]. The presence of long linear grooves on its surface supports this, as such features are typically associated with cracks that require a level of structural coherence, which would be absent in asteroids lacking internal integrity [12]. Thus, the identification of similar features on Didymos upon Hera's arrival would strongly support the hypothesis of internal rigidity as a plausible explanation.

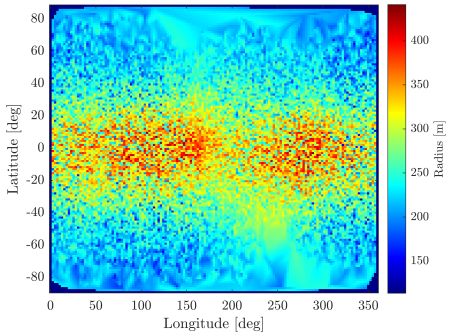

Fig. 4. **C7**: Maps of the radius of the aggregate.

5.2 Angular momentum and spin rate

In terms of angular momentum, a noticeable trend emerges with a gradual decrease over time. This reduction is primarily due to interactions among the fragments within the aggregate. Moreover, Figure 5 shows a significant disparity in momentum loss, particularly evident in the scenario without a core, where losses reach approximately 23%, compared to a mere 2.8% in the rigid core

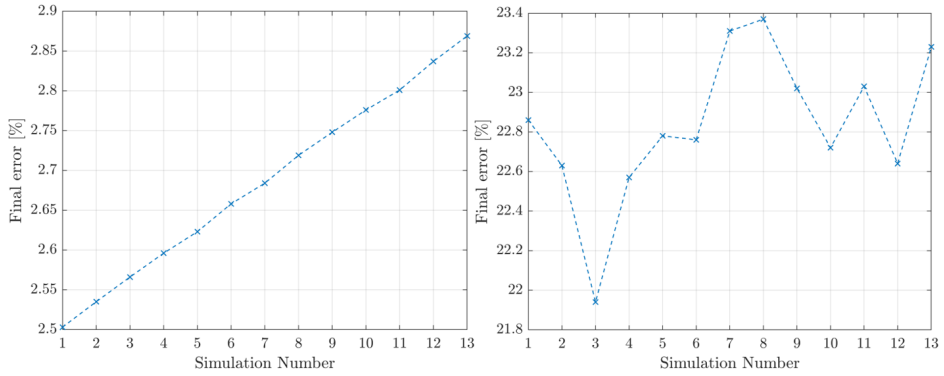

Fig. 5. Angular momentum loss comparison between *C* and *N* simulations.

case. Additionally, other trends are highlighted in percentage comparisons across simulations. While simulations with a rigid core display a linear increase in the difference between initial and final angular momentum values with increasing internal density, no clear trend is evident in the non-rigid core scenario. However, the *N* evolution correlates with the pattern of mass loss, where greater mass loss corresponds to a higher loss of angular momentum due to changes in aggregate moments of inertia.

This loss of angular momentum results in a reduction in the spin rate of the aggregate, particularly evident in the scenario without a core, see Figure 15. Here, an initial oscillatory adjustment phase is observed, likely caused by the initial compaction induced by the simulation's outset, which alters the aggregate's inertia. This compression is more pronounced initially in the non-rigid core scenario due to a larger volume of empty space between particles, facilitating more effective gravitational compression.

5.3 Contact forces

Another crucial aspect in the study of aggregate evolution concerns the contact forces between particles, with particular attention to both rigid core and non-core models. The temporal evolution of mean contact forces, represented in Figures 6 and 7, shows an initial phase of oscillations, mirroring trends observed in the asteroid's spin rate. In both core and non-core scenarios, force peaks occur at the beginning of the simulation, but differ in magnitude and distribution. As graphically depicted in Figures 16 and 17, analyzing the contacts at the initial, final and peak time offers further insights:

- **C**: In the core model, the highest contact forces are concentrated around the rigid core in the final phase, while the initial distribution is more uniform across the aggregate. This indicates that the core stabilizes the structure, with the inner particles bearing the greatest forces as the system evolves.
- **N**: Peak occurs shortly after the start, reaching higher magnitudes, suggesting a more compact final aggregate than the initial scenario. In addition, the contact force distribution is initially uniform but becomes concentrated in the mid-range radius as compression builds. The final stage displays a triangular distribution, with forces peaking halfway between the center and edge of the aggregate.

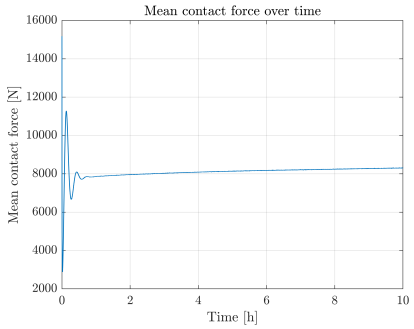

Fig. 6. **C7**: Mean contact forces evolution.

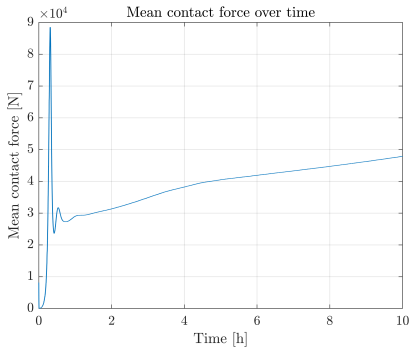

Fig. 7. **N7**: Mean contact forces evolution.

Additionally, in scenarios without a core, maximum contact forces consistently occur at the poles. At the equator, a band of minimal forces is formed over a latitude range of about ±20 degrees, reflecting regions of reduced interaction. This distribution is consistent with prior observations of asteroid Bennu [9], where gravitational forces are counterbalanced by rotational centrifugal forces at the equator, leading to equatorial bulging.

5.4 Particle displacements

A particular emphasis is placed on the internal dynamical behaviour and the evolution of particle distributions, aiming at identifying patterns of movement that enhance the understanding of rubble-pile asteroids.

To quantify particle displacement, the aggregate system's geometric center (G.C.) was used as the origin of the reference frame. The initial and final radii of particles relative to the G.C. were calculated, and their differences provided a measure of individual particle displacements. A radial analysis was conducted by dividing particles into radial zones of approximately 3 meters, providing information about the direction and magnitude of particle movement, as illustrated in Figures 8 and 9.

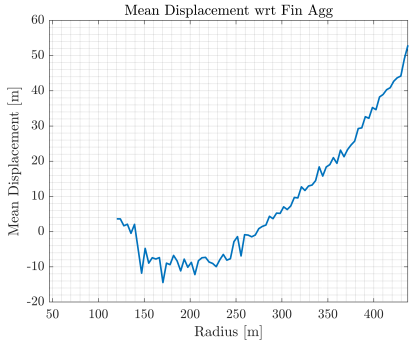

Fig. 8. **C**: Mean displacements analysis.

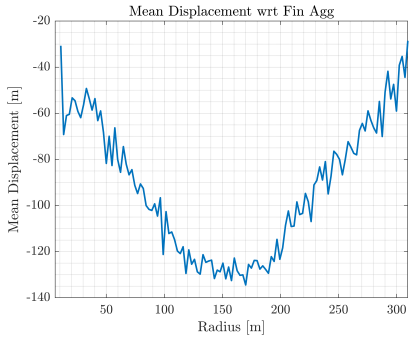

Fig. 9. **N**: Mean displacements analysis.

In case *C*, particles initially located near the surface tend to migrate outward, while those positioned closer to the core show minimal displacement. This suggests an overall expansion of the aggregate, with an observed stabilization effect from the rigid core. The final positions confirm this trend, with the most significant outward displacements occurring among particles farther from the core, particularly those situated at the outermost layers of the aggregate. In contrast, case *N* shows a general inward movement of particles across all layers, indicating aggregate compression. Interestingly, particles near the midpoint of the radial distance exhibit internal mixing, as those closer to the center move outward while those farther out shift inward.

Detailed maps of particle displacements further revealed distinct regional patterns. In case *C*, compression at the poles leads to particles moving closer together, whereas equatorial particles are pushed outward. In case *N*, material is ejected in regions with bulging surfaces, primarily at the equator, where particles also tend to migrate inward in areas without bulging. Density played a critical role in particle dynamics, particularly in case *C*. Higher densities of the rigid core caused particles closer to the core to move outward, while those located further from the center showed slight inward movement, suggesting a remixing effect.

To further investigate particle displacements, test particles were considered at various radii within the aggregate, numbered from 1 to 10 based on their increasing initial distance from the center, as depicted in Figures 18, 19 and 20. Their trajectories, tracked over time, highlighted significant differences between the two cases. In case *C*, the trajectories appear regular with well-defined periodicity. Particularly, examining the innermost particles reveals a distinct pattern passing through four well-defined locations that recur periodically, see Figure 10. As the initial radius increases, there is a tendency towards a more circular trajectory around the geometric center. Similarly, in case *N*, there is a trend towards more circular orbits at larger initial radii, as shown in Figure 11. However, unlike case *C*, the internal orbits exhibit more complex evolutions, although a certain periodicity can still be discerned.

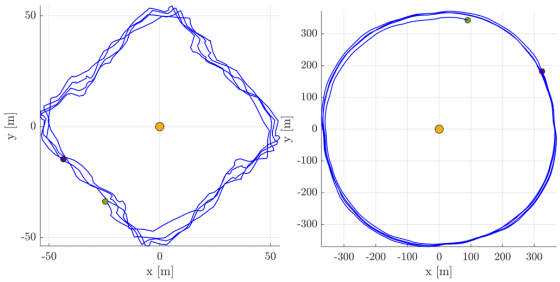

Fig. 10. **C**: Test particles 1 and 9 evolutions with respect to the G.C.

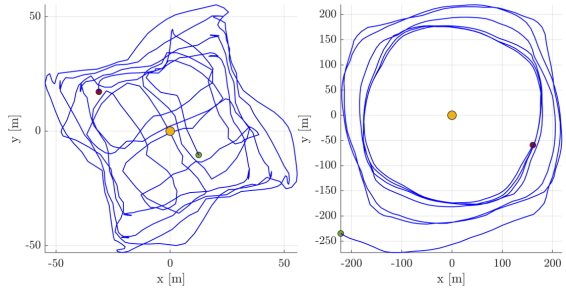

Fig. 11. **N**: Test particles 1 and 9 evolutions with respect to the G.C.

To clarify the observed phenomena, an investigation was conducted into the sources of periodicity by tracking the evolution of the system's G.C. and barycenter. The barycenter followed a linear path in the inertial system, while the G.C. rotated around it, revealing periodic patterns. Transitioning to the reference frame relative to the G.C., specific patterns become evident, as depicted in Figure 21. Frequency analyses relative to the aggregate's geometric center revealed resonance frequencies between the barycenter and G.C. influencing particle behaviour. The test particles closer to the center were more influenced by higher resonance frequencies, while the outer particles were dominated by lower frequencies.

In case *C*, the barycenter remained relatively stable, with the G.C. exhibiting periodic motion around it. This interaction was found to influence particle dynamics, contributing to periodic resonance patterns observed in the frequency analysis. In case *N*, where the barycenter was more offset due to mass loss, the evolution of particle trajectories became more complex, leading to greater mixing of inner particles. Overall, the analysis underscores the stabilizing influence of a rigid core in rubble-pile asteroids and highlights the significance of barycenter dynamics in shaping particle displacement patterns.

5.5 Density distributions

Finally, moving on to the density analysis, *C* simulations are characterized by alterations only in the density of the rigid core, making these cases irrelevant. Conversely, in aggregates without a rigid core, several particles have altered densities. To better understand the distribution of these density layers within the final aggregate, correlating particle positions by radius relative to the G.C. proved valuable. Preliminary evaluations indicate that particles with altered density, initially located within an internal volume, remain within the aggregate, consistent with the displacement analysis. Notably, in the case without a core, examining the density distribution in latitude and longitude through layered maps reveals that some internal particles move toward the surface, particularly where the aggregate elongates, while remaining within the structure. Additionally, in cases with an underdense core, particles forming the core appear more compact and less infiltrated by particles of different densities compared to aggregates with denser cores, see Figures 12 and 13.

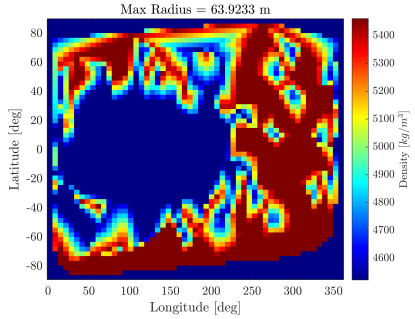

Fig. 12. **N1**: Density distribution layered maps in the final aggregates.

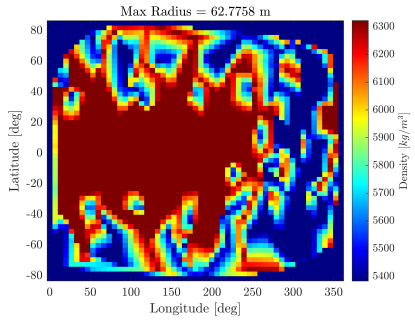

Fig. 13. **N13**: Density distribution layered maps in the final aggregates.

6. Conclusions

The investigation into the properties and dynamical evolution of Didymos has provided valuable insights into the intricate relationship between its internal structure and density distribution. This chapter synthesizes the key findings, presenting a comprehensive overview of the study's implications and contributions. Furthermore, it offers a glimpse into potential further exploration and development within the scope of this research.

6.1 Summary of the results

The simulations have demonstrated that the presence of a rigid core plays a critical role in the evolution of Didymos. The core provides a stabilizing effect, reducing momentum loss, asymmetrical deformations and mitigating mass loss. Notably, the core introduces interesting structural features, such as a groove crossing the aggregate, which highlights the structural complexity of rubble-pile asteroids and suggests potential parallels with observed asteroidal morphology.

The different density distributions have also influenced the evolution of the aggregates in both cases. In the cases with a rigid core, this results in a decrease in flattening with increasing internal density. Conversely, an inverse correlation between oblateness and mass loss has been identified in structurally homogeneous cases, indicating that aggregates experiencing greater mass loss tend to exhibit lower oblateness and reduced flattening. Both aggregate configurations show polar flattening, with a more noticeable effect in cases without a rigid core. Thus, if a rigid core is present, it could become exposed under certain conditions.

The analysis of contact forces revealed notable patterns during the transient phase, marked by oscillations in force values and peaks. In scenarios without a core, forces concentrated at the poles, while equatorial regions exhibited bulging and minimal forces, highlighting the intricate balance between gravitational attraction and centrifugal forces during the asteroid's rotational dynamics.

The study of particle displacements revealed key differences in material rearrangement within the aggregates. In scenarios with a rigid core, the core reduced inward displacements, leading to more stable particle trajectories. In contrast, coreless aggregates experienced more complex particle movements due to mass loss. Additionally, the movement of the system's barycenter was found to influence the motion of particles deeper within the aggregate.

Finally, the investigation of density distribution confirmed that internal density affects the final arrangement of particles. Scenarios with non-rigid underdense cores showed a more compact internal structure than those with denser cores. Additionally, the lower average particle displacement around the underdense core in rigid cases suggests that these aggregates are more resistant to mixing phenomena.

6.2 Future developments

Given the susceptibility of the analyzed problem to various simulation-level influences, potential enhancements in the problem setup are crucial. These include:

- Extending simulation timeframes to explore Didymos aggregates' dynamic evolution over longer periods.
- Increasing the number of simulations to enhance statistical significance.
- Varying the size of the internal core for additional insights.
- Introducing external forces like solar radiation pressure to simulate the YORP effect.
- Including Dimorphos in the simulation's environment.
- Incorporating ejecta's impact scenarios from the DART mission.
- Conducting experimental research in microgravity to validate outcomes.

Additionally, subsequent comparison with ESA's Hera mission data would address initial assumptions' uncertainties.

References

[1] H. Karttunen, P. Kröger, H. Oja, M. Poutanen, and K. J. Donner, *Fundamental Astronomy*. Springer, 2017.

[2] NASA JPL CNEOS. "NEO Basics - NEO Groups." (2024), [Online]. Available: `https://cneos.jpl.nasa.gov/about/neo_groups.html` (visited on 08/30/2024).

[3] NASA JPL CNEOS. "NEO Search Program." (2024), [Online]. Available: `https://cneos.jpl.nasa.gov/about/search_program.html` (visited on 08/30/2024).

[4] A. Cheng, H. Agrusa, B. Barbee, A. Meyer, T. Farnham, and S. Raducan et al., "Momentum Transfer from the DART Mission Kinetic Impact on Asteroid Dimorphos," *Nature 616*, pp. 457–460, 2023.

[5] D. Richardson, Z. Leinhardt, J. Melosh, W. Bottke, and E. Asphaug, "Gravitational Aggregates: Evidence and Evolution," *Asteroids III*, 2002.

[6] Y. Zhang, D. C. Richardson, O. S. Barnouin, P. Michel, S. R. Schwartz, and R.-L. Ballouz, "Rotational Failure of Rubble-pile Bodies: Influences of Shear and Cohesive Strengths," *The Astrophysical Journal, 857*, p. 15, 2018.

[7] F. Ferrari and E. M. Alessi, "A new method for identifying dynamical transitions in rubble-pile asteroid scenarios," *Astronomy & Astrophysics, 672*, A35, 2023.

[8] Y. Zhang *et al.*, "Inferring interiors and structural history of top-shaped asteroids from external properties of asteroid (101955) Bennu," *Nature Communications, 13*, 2022.

[9] D. J. Scheeres *et al.*, "Heterogeneous mass distribution of the rubble-pile asteroid (101955) Bennu," *Science Advances, 6*, no. 41, 2020.

[10] M. Hirabayashi *et al.*, "The Western Bulge of 162173 Ryugu Formed as a Result of a Rotationally Driven Deformation Process," *The Astrophysical Journal Letters, 874*, p. L10, 2019.

[11] S. Naidu *et al.*, "Radar observations and a physical model of binary near-Earth asteroid 65803 Didymos, target of the DART mission," *Icarus, 348*, p. 113 777, 2020.

[12] O. Barnouin *et al.*, "Shape of (101955) Bennu indicative of a rubble pile with internal stiffness," *Nature Geoscience, 12*, p. 1, 2019.

[13] Y. Zhang *et al.*, "Creep stability of the proposed AIDA mission target 65803 Didymos: I. Discrete cohesionless granular physics model," *Icarus, 294*, pp. 98–123, 2017.

[14] F. Ferrari and P. Tanga, "Interior of top-shaped asteroids with cohesionless surface," *Icarus, 378*, p. 114 914, 2022.

[15] D. J. Scheeres, "Minimum energy configurations in the N-body problem and the celestial mechanics of granular systems," *Celestial Mechanics and Dynamical Astronomy, 113*, pp. 291–320, 2012.

[16] D. J. Scheeres, "Hill Stability of Configurations in the Full N-Body Problem," *Asteroids: New Observations, New Models, 318*, pp. 128–134, 2016.

[17] D. J. Scheeres, "Stability of the Euler resting N-body relative equilibria," *Celestial Mechanics and Dynamical Astronomy, 130*, p. 26, 2018.

[18] D. J. Scheeres, "Minimum energy asteroid reconfigurations and catastrophic disruptions," *Planetary and Space Science,57*, pp. 154–164, 2009.

[19] D. J. Scheeres, "Disassociation energies for the finite-density N-body problem," *Celestial Mechanics and Dynamical Astronomy, 132*, p. 4, 2020.

[20] F. Ferrari, A. Tasora, P. Masarati, and M. Lavagna, "N-body gravitational and contact dynamics for asteroid aggregation," *Multibody System Dynamics, 39*, pp. 3–20, 2017.

[21] F. Ferrari, M. Lavagna, and E. Blazquez, "A parallel-GPU code for asteroid aggregation problems with angular particles," *Monthly Notices of the Royal Astronomical Society, 492*, pp. 749–761, 2019.

[22] Johns Hopkins APL. "Outreach - DART 3D Printable Models." (2024), [Online]. Available: `https://dart.jhuapl.edu/Outreach/index.php` (visited on 01/30/2024).

Appendix A: Initial Data

Table 2 provides information on the properties of the initial aggregates, where V_{fil} is the actual volume filled with material and V_{tot} is the volume of the convex envelope. More details on the physical meaning of the parameters listed in the table are provided in the equations below. The porosity of the aggregate is defined as in Equation 1. The characteristic lengths are defined as the dimensions with respect to the inertial frame. While the radii measures describe the three main dimensions of the aggregate regardless of the direction of the x and y axes. Indeed, they are computed as in Equation 2, where $\mathbf{r}_{xy}$ contains the radii in the $x-y$ plane and z_L is the characteristic length along the z axis. Table 2 also presents α_1, which is the aspect ratio of the models. Thus, it is a measure of how stretched or flattened the asteroid is along its principal axes. This is defined as the ratio of the shortest semi-axis (r_3) to the longest semi-axis (r_1), see Equation 3, while α_2 analyze only the components on the $x-y$ plane. Additionally, the value of the oblateness (O) is also provided.

Finally, the parameters related to the surface properties are presented in Table 3. These define the material characteristics and interaction dynamics used in the numerical simulations to accurately model the asteroid's behaviour, including Young's modulus (E), Poisson's ratio (v), restitution coefficient (e), static friction coefficient (μ_s), sliding friction coefficient (μ_k), normal stiffness coefficient (K_n), tangential stiffness coefficient (K_t), normal damping coefficient (G_n), and tangential damping coefficient (G_t).

	Rigid Core	No Rigid Core
Number of particles	5973	6455
Characteristic lengths (x,y,z) [m]	799.883, 785.696, 608.207	814.705, 796.874, 602.749
Radii ($\max_{xy}$, $\min_{xy}$, z) [m]	413.538, 389.124, 304.103	416.380, 361.686, 301.375
Oblateness	0.265	0.276
α_1	0.735	0.724
α_2	0.941	0.869
V_{fil} [m^3]	1.343×10^8	1.108×10^8
V_{tot} [m^3]	2.037×10^8	2.037×10^8
Porosity (Φ)	0.340	0.456
Total mass [kg]	6.009×10^{11}	6.009×10^{11}
Material density [kg/m^3]	4472.841	5422.020
Bulk density [kg/m^3]	2950	2950

Table 2. Shape models geometrical characteristics and material properties.

$$\Phi = 1 - \frac{V_{fil}}{V_{tot}} \quad [1]$$

$$r_1 = max(\mathbf{r}_{xy}) \qquad r_2 = min(\mathbf{r}_{xy}) \qquad r_3 = \frac{z_L}{2} \quad [2]$$

$$O = \frac{r_1 - r_3}{r_1} \qquad \alpha_1 = \frac{r_3}{r_1} \qquad \alpha_2 = \frac{r_2}{r_1} \quad [3]$$

E [Pa]	v	e	μ_s	μ_k	Adhesion [Pa]	K_n	K_t	G_n	G_t
3×10^9	0.3	0	0.6	0.6	0	200000	200000	40	20

Table 3. Surface properties.

Appendix B: Additional Results

Final shape configurations

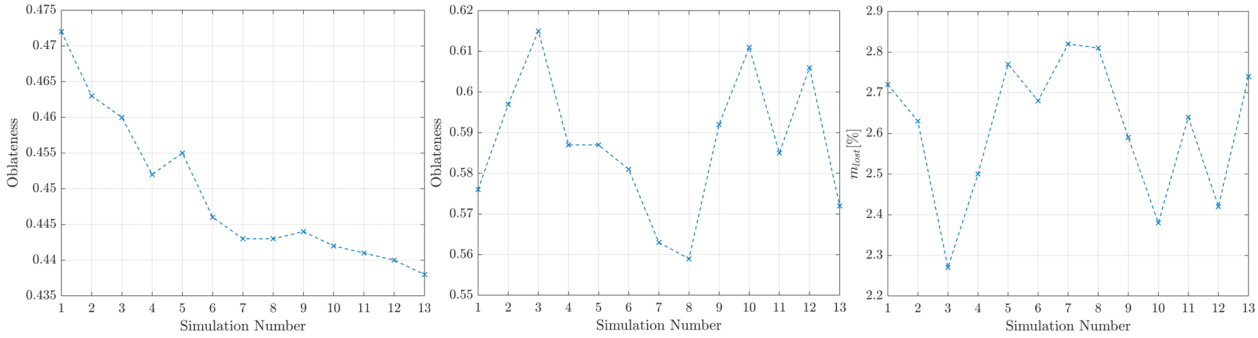

Fig. 14. Oblateness comparison between *C* and *N* final aggregates and mass shedding percentage over all *N* simulations.

Spin rate

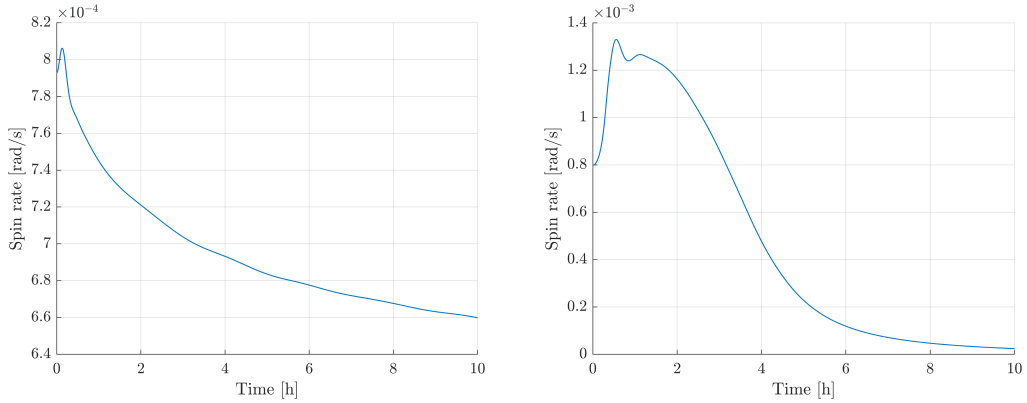

(a) Aggregate with an inner rigid core.

(b) Aggregate without an inner rigid core.

Fig. 15. Spin rate evolution of the nominal cases.

Contact forces

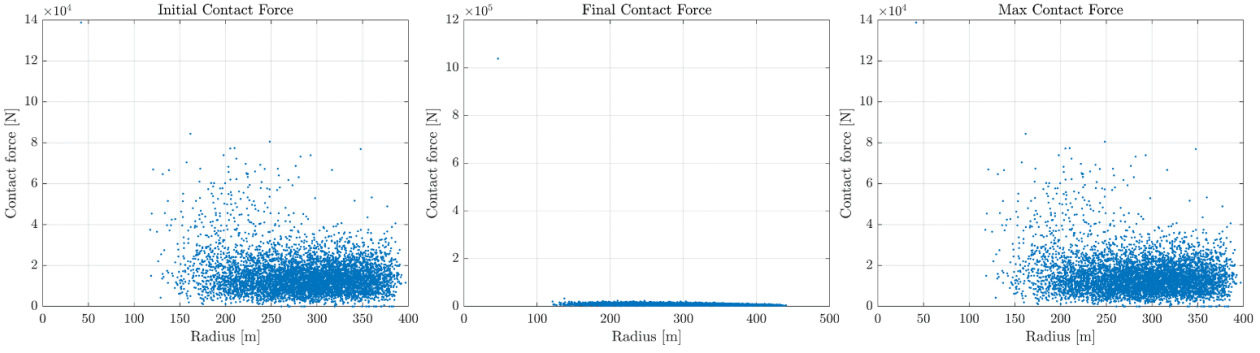

Fig. 16. **C**: Contact forces distributions at different times.

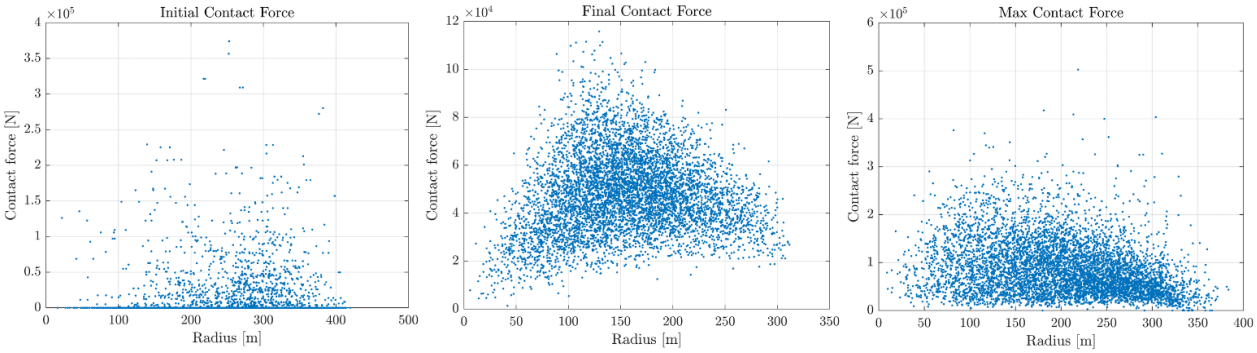

Fig. 17. **N**: Contact forces distributions at different times.

Particle displacements

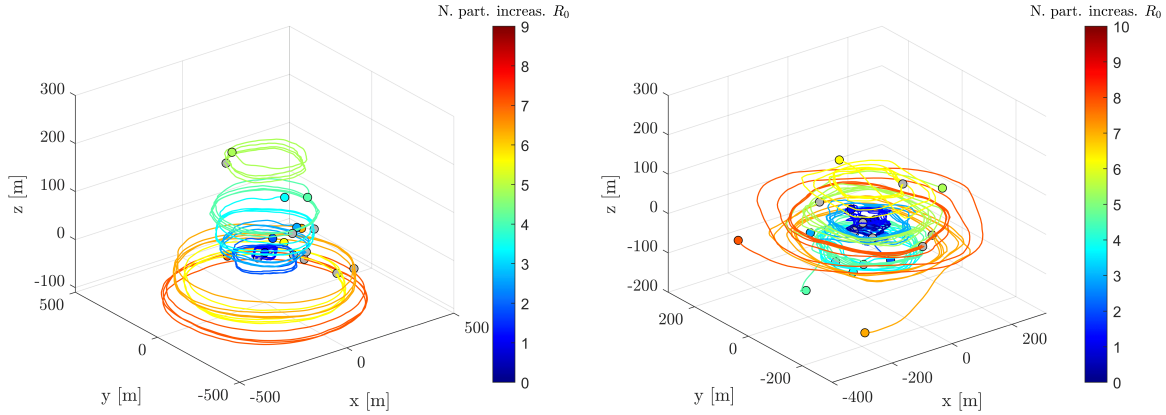

(a) Aggregate with an inner rigid core.

(b) Aggregate without an inner rigid core.

Fig. 18. Evolution of all test particles with respect to the G.C.

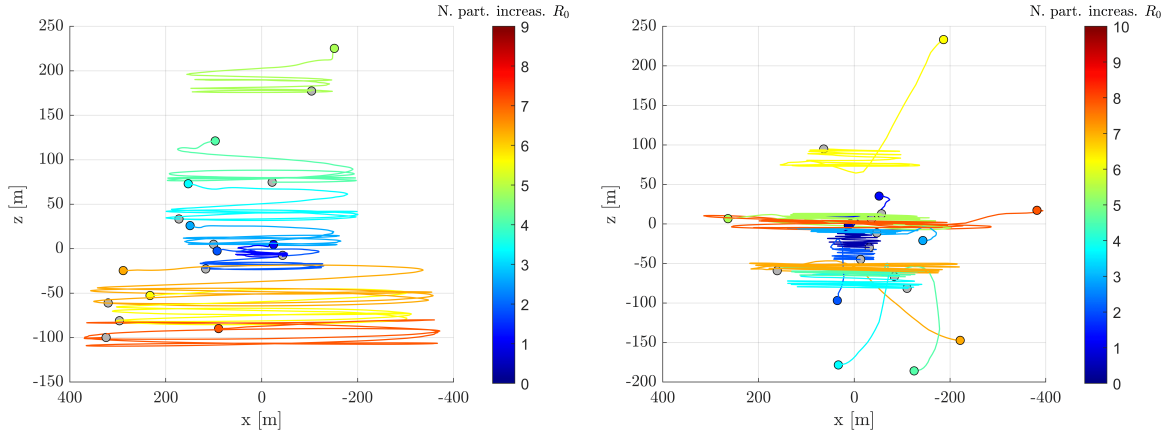

(a) Aggregate with an inner rigid core.

(b) Aggregate without an inner rigid core.

Fig. 19. Evolution of all test particles with respect to the G.C. in lateral view.

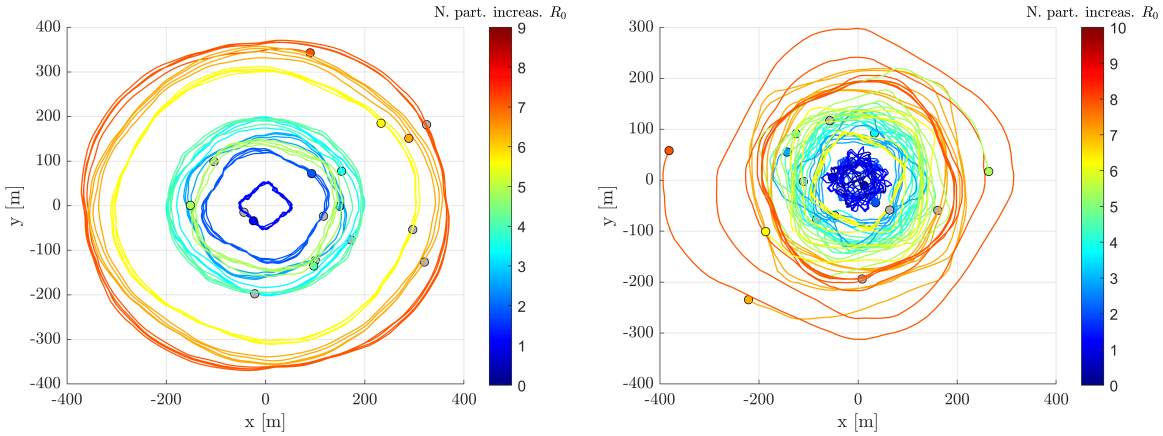

(a) Aggregate with an inner rigid core.

(b) Aggregate without an inner rigid core.

Fig. 20. Evolution of all test particles with respect to the G.C. in up view.

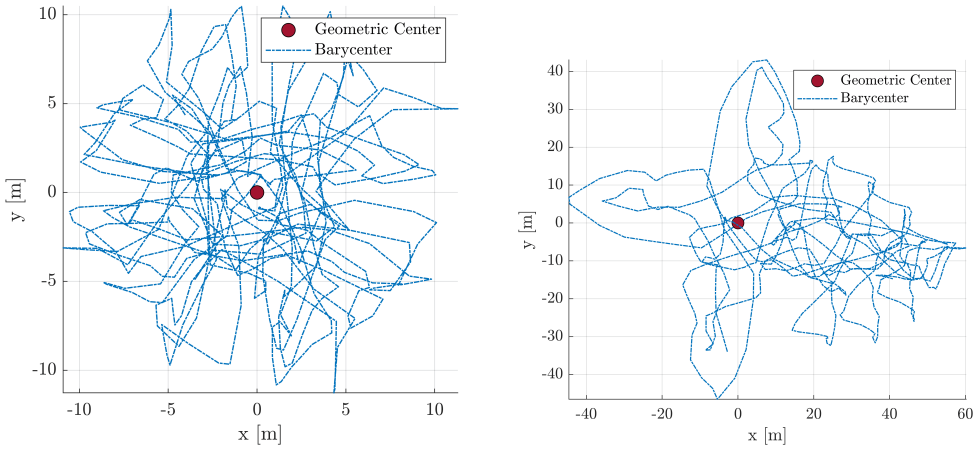

(a) Aggregate with an inner rigid core.

(b) Aggregate without an inner rigid core.

Fig. 21. Barycenter evolution with respect to the geometric center of the aggregate.